Physics Letters B 791 (2019) 414–419

Contents lists available at ScienceDirect

Physics Letters B

www.elsevier.com/locate/physletb

Fate of the neutron–deuteron virtual state as an Efimov level

Gautam Rupak [a,*], Akshay Vaghani [a], Renato Higa [b], Ubirajara van Kolck [c,d]

[a] Department of Physics & Astronomy and HPC[2] Center for Computational Sciences, Mississippi State University, Mississippi State, MS 39762, USA
[b] Instituto de Física, Universidade de São Paulo, R. do Matão 1371, 05508-090, São Paulo, SP, Brazil
[c] Institute de Physique Nucléaire, CNRS/IN2P3, Université Paris-Sud, Université Paris-Saclay, 91406 Orsay, France
[d] Department of Physics, University of Arizona, Tucson, AZ 85721, USA

ARTICLE INFO

Article history:
Received 7 June 2018
Received in revised form 8 August 2018
Accepted 27 August 2018
Available online 7 September 2018
Editor: W. Haxton

Keywords:
Efimov levels
Neutron–deuteron scattering
Nuclear effective field theory

ABSTRACT

The emergence of Efimov levels in a three-body system is investigated near the unitarity limit characterized by a resonant two-body interaction. No direct evidence of Efimov levels is seen in the three-nucleon system since the triton is the only physical bound state. We provide a model-independent analysis of nucleon–deuteron scattering at low energy by formulating a consistent effective field theory. We show that virtual states evolve into shallow bound states, which emerge as excited triton levels as we drive the system towards unitarity. Even though we consider this specific system, our results for the emergence of the Efimov levels are universal.

1. Introduction

A distinctive feature of three-body physics is the Efimov effect [1–4]. In the presence of resonant two-body scattering, the three-body system supports a tower of bound states whose binding energies display geometric scaling. The number of three-body bound states was predicted to scale as $\ln(a_0/r_0)$, where a_0 is the resonating two-body s-wave scattering length, and $r_0 \ll a_0$ is the range of the interaction. Experimental verification through the detection of excited states was provided three decades later in cold-atom experiments [5–9], where the ratio a_0/r_0 could be increased by varying magnetic fields near a Feshbach resonance.

Recently, the first excited Efimov state was identified [10] for atomic ^{4}He, where a_0/r_0 is sufficiently large even in the absence of external magnetic fields. In complex nuclei the ratio a_0/r_0 is often unknown, but in some cases it might be large enough to accommodate an excited state: halo nuclei such as ^{11}Li, ^{22}C, or even as heavy as ^{62}Ca, where two neutrons are weakly bound to a tight nuclear core, provide opportunities to observe the Efimov effect [11–13].

Neutron–deuteron (nd) at low energy is another system that could provide evidence of Efimov physics. Low-energy scattering is dominated by s waves with spins $S = 3/2$ (quartet) and $S = 1/2$ (doublet). In the quartet channel, where spins are aligned, the Pauli exclusion principle prevents a three-nucleon (3N) bound state. In the doublet channel, the strong nuclear force leads to an attractive interaction that supports a 3N bound state, the triton (^{3}H) with a binding energy $B_3 \simeq 8.48$ MeV. The next deeper Efimov state would appear only at ~ 4 GeV, beyond the regime where a description in terms of nucleons makes sense. Here we search for a remnant of the next *shallower* Efimov state.

The low-energy phase shift in the doublet channel was analyzed by van Oers and Seagrave [14], who suggested a modified effective range expansion (ERE) to describe the data below the deuteron breakup momentum. The presence of a virtual state with binding energy $\simeq 0.515$ MeV was inferred [15]. Adhikari et al. [16] showed in a separable potential model that this virtual state is related to the Efimov spectrum. A similar connection for ^{20}C [17,18] and for atomic systems [19] was investigated within a zero-range model.

In contrast, we use the effective field theory (EFT) formalism to provide a model-independent analysis of the nd system at low energies. All interactions allowed by symmetries are constructed with the relevant low-energy degrees of freedom, without modeling the high-energy physics. A systematic scheme for calculations is formulated by expressing observables as an expansion in the small ratio p/Λ_b, where p is a typical low momentum scale associated with the processes of interest and Λ_b is a high momentum scale that marks the breakdown of the EFT.

In the so-called pionless EFT ($\not\pi$EFT) the relevant degrees of freedom are nonrelativistic nucleons (and other light particles such

* Corresponding author.
E-mail address: grupak@ccs.msstate.edu (G. Rupak).

https://doi.org/10.1016/j.physletb.2018.08.051

as photons, electrons and neutrinos) with $\Lambda_b \sim m_\pi$, the pion mass, associated with the pion physics that is not included explicitly. $\not\pi$EFT has been very successful in describing two- and three-nucleon systems — see for example Refs. [20–27] — when the typical momentum is taken to be $p \sim \gamma \sim a_t^{-1}$, with $\gamma \simeq 45.7$ MeV the deuteron binding momentum and $a_t \simeq 5.4$ fm the scattering length in the two-nucleon (2N) $^3S_1$ channel.

EFT enables us to study *nd* scattering in the limit $a_t \to \infty$, where the 2N scattering amplitude is only bounded by unitarity. We first fit the parameters of $\not\pi$EFT to reproduce the relevant 2N and 3N experimental data. $\not\pi$EFT is then treated as the underlying theory that is used to generate artificial "data" at increasingly large values of a_t. We develop a new low-energy EFT, which we refer to as halo EFT, to provide a model-independent analysis of the 3N phase shift at low momentum generated from $\not\pi$EFT. This halo EFT, which treats the deuteron as an "elementary" particle and is thus applicable only below the deuteron breakup, is modeled after other halo EFTs where different clusters of nucleons are treated as relevant degrees of freedom [28,29]. Here, the deuteron is the core and the neutron forms the "halo" around it, consisting of shallow virtual and bound states. The halo EFT provides a theoretical basis for the modified ERE obtained empirically by van Oers and Seagrave, and allows us to track the virtual state at unphysical scattering lengths. As we drive $\not\pi$EFT towards the unitarity limit, the binding energy of the virtual state decreases till it becomes the first excited bound state of the triton, thus demonstrating its Efimov character. Higher Efimov states appear in the same way if the scattering lengths are increased further. Although we focus on the 3N system, our framework could be applied to study the emergence of Efimov levels in other systems as well.

2. Pionless EFT

The doublet *nd* scattering amplitude was first calculated at leading order (LO) in $\not\pi$EFT in Ref. [22]. It receives contributions from the LO 2N interactions, which consist of a single non-derivative contact operator in each 2N s wave ($^3S_1$ and $^1S_0$) with strength determined in terms of the respective scattering length. In addition, there is a contribution from a 3N non-derivative contact interaction, which is needed to render the amplitude well-defined. Next-to-leading-order (NLO) corrections introduce a two-derivative interaction in each 2N s wave, which can be constrained by the corresponding effective range. No new 3N interaction contributes at this order [22,24]. A momentum-dependent 3N interaction enters at NNLO [25]. To this order, the EFT expansion has been shown to be convergent [26], and to reproduce both experimental data (when available) and results from sophisticated phenomenological potentials.

The unitarity limit corresponds not only to arbitrarily large 2N scattering lengths but also to vanishing 2N effective ranges and higher ERE parameters. This removes higher-order corrections in the 2N interaction. Higher-order 3N forces are less important for 3N states shallower than the triton. A LO calculation is sufficient to explore the connection to the Efimov spectrum. The LO *nd* T-matrix $T_t(p) = 8\pi\gamma_t A_t(p,p)/m_N$ is obtained from two coupled integral equations [22]:

$$
\begin{aligned}
A_t(k,p) &= \frac{1}{4}\Big[\mathcal{K}(k,p) + h_0(\lambda)\Big] \\
&\quad + \int_0^\lambda \frac{dqq^2}{2\pi}\Big\{\Big[\mathcal{K}(k,q) + h_0(\lambda)\Big]\mathcal{D}_t(E - \frac{q^2}{2m_N}; q)A_t(q,p) \\
&\quad + \Big[3\mathcal{K}(k,q) + h_0(\lambda)\Big]\mathcal{D}_s(E - \frac{q^2}{2m_N}; q)A_s(q,p)\Big\}, \\
A_s(k,p) &= \frac{1}{4}\Big[3\mathcal{K}(k,p) + h_0(\lambda)\Big] \\
&\quad + \int_0^\lambda \frac{dqq^2}{2\pi}\Big\{\Big[3\mathcal{K}(k,q) + h_0(\lambda)\Big]\mathcal{D}_t(E - \frac{q^2}{2m_N}; q)A_t(q,p) \\
&\quad + \Big[\mathcal{K}(k,q) + h_0(\lambda)\Big]\mathcal{D}_s(E - \frac{q^2}{2m_N}; q)A_s(q,p)\Big\}, \\
\mathcal{K}(k,q) &= \frac{1}{kq}\ln\left(\frac{k^2+kq+q^2-m_N E - i0^+}{k^2-kq+q^2-m_N E - i0^+}\right),
\end{aligned}
\tag{1}
$$

where $E = 3p^2/(4m_N) - \gamma_t^2/m_N$ is the total center-of-mass energy and $m_N \simeq 938.9$ MeV is the isospin-averaged nucleon mass. The intermediate 2N contribution is contained in the two-point Green's function $\mathcal{D}_\eta(E;p) = (-\gamma_\eta + \sqrt{-m_N E + p^2/4 - i0^+})^{-1}$, where $\eta = t$ (s) for the $^3S_1$ ($^1S_0$) channel. In the $^3S_1$ channel we use the deuteron binding momentum to set $\gamma_t = g_t\gamma$, and in the $^1S_0$ channel, where no bound state exists, we use the scattering length $a_s \simeq -23.714$ fm to fix $\gamma_s = g_s/a_s$, which is consistent with the LO power counting [20,30]. The physical point corresponds to $g_t = g_s = 1$. The $3N$ amplitudes $A_{t,s}$ do not converge when the regulator is removed, $\lambda \to \infty$, unless we fix the 3N parameter $h_0(\lambda)$ to guarantee that one 3N observable is made regulator independent. For any given cutoff λ, we tune h_0 such that we reproduce the doublet scattering length $a_3 = 0.65$ fm [31] for $g_t = g_s = 1$. This determines the independent parameter $\Lambda_\star$ appearing in the log-periodic 3N force [22].

The doublet phase shift is obtained from $p\cot\delta = ip + 2\pi/[\mu T_t(p)]$, with $\mu \approx 2m_N/3$ the *nd* reduced mass. In Fig. 1, we show the phase shift calculated from the three-body integral equations in Eq. (1) at the physical point and a few results as we approach the unitarity limit. The only physical parameters that enter the microscopic calculation using $\not\pi$EFT are g_t, g_s, and $\Lambda_\star$. We approach unitarity taking $g_s = 0$ and making the deuteron arbitrarily shallow, $g_t \to 0$, while keeping $\Lambda_\star$ fixed.

For short-ranged interactions, $p\cot\delta$ is an analytic function of p^2. However, $p\cot\delta$ rises rapidly at low momenta — see panel (a) of Fig. 1 — and for $g_t = g_s = 1$ a simple Taylor series expansion around $p = 0$ gives a poor description even at relatively small momenta $p \sim 10$ MeV. Instead, the modified ERE [14]

$$
\begin{aligned}
p\cot\delta &= \frac{-1/a + rp^2/2 + sp^4/4 + \cdots}{1 + p^2/p_0^2} \\
&= -\frac{R}{1+p^2/p_0^2} - A + Bp^2 + \cdots,
\end{aligned}
\tag{2}
$$

works remarkably well up to about the deuteron breakup momentum $2\gamma/\sqrt{3} \simeq 53$ MeV. While bound and virtual states correspond to poles of the T-matrix $T_t(p)$ at imaginary momenta $p = i\kappa_j$, there is also a pole in $p\cot\delta$ at $p^2 = -p_0^2$ that corresponds to a zero of $T_t(p)$. When we fit the modified ERE to the LO phase shift in panel (a) of Fig. 1, we get the fit parameters $a \approx 0.65$ fm $= a_3$, $r \approx -141$ fm, $s \approx 62$ fm^3, and $p_0 \approx 16.1$ MeV, which translate into a shallow virtual state at $\kappa_1 \approx -26.8$ MeV with a binding energy ≈ 0.574 MeV. Naively one might expect all the scattering parameters to scale with some power of the range of nuclear interaction $\sim m_\pi^{-1} \simeq 1.4$ fm. The fitted parameters p_0^{-1}, a^{-1} and r are unusually large compared to the naive expectation. The standard ERE holds only for $p \ll p_0$, with large inverse scattering length a^{-1}, effective range $r + 2(ap_0^2)^{-1}$, *etc.*

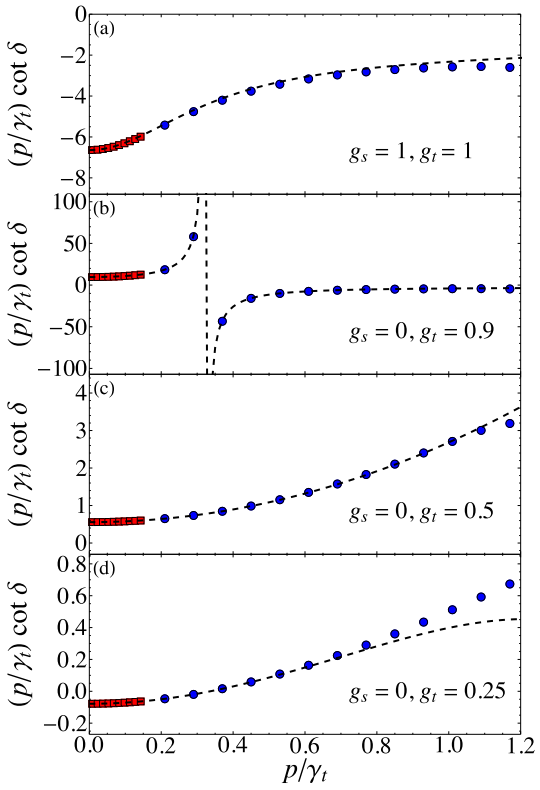

Fig. 1. Phase shift: $p\cot\delta$ as function of the momentum p, both in units of the deuteron binding momentum γ_t. The (blue) dots and (red) squares are numerical results from solving Eq. (1) for several values of g_t, g_s as indicated, once the 3N parameter $\Lambda_\star$ is determined by imposing $a_3 = 0.65$ fm for $g_t = g_s = 1$. The (black) dashed curves are modified ERE fits to the data over a small momentum range indicated as (red) squares. We expect the modified ERE fits to describe the numerical results for $p/\gamma_t \lesssim 2/\sqrt{3}$. (For interpretation of the colors in the figure(s), the reader is referred to the web version of this article.)

3. Halo EFT and modified ERE

We now formulate the halo EFT that describes *nd* scattering below the deuteron breakup momentum $2\gamma_t/\sqrt{3}$, and provides a justification for Eq. (2). In this theory the deuteron is treated as a fundamental particle, and so the breakup momentum sets the breakdown scale $\Lambda_b \sim \gamma_t$. A shallow s-wave pole by itself can be accounted for in the standard ERE by a large scattering length such as in the 2N $^1S_0$ and $^3S_1$ channels, requiring a fine-tuned interaction to be treated nonpertubatively at LO [20,30]. A shallow amplitude zero by itself requires another fine-tuning that leads to a perturbative amplitude with a large effective range and a small scattering length [30]. Here we identify two momentum scales associated with the presence of both zero and virtual pole, respectively $|p_0| \sim Q$ and $|\kappa_1| \sim \aleph$. The parameters a, r and p_0 are fine-tuned, and we require three fine-tuned couplings to reproduce the desired modified ERE. The halo EFT is conveniently written using two auxiliary fields as

$$\begin{aligned}\mathcal{L} =& n^\dagger\left(i\partial_0 + \frac{\nabla^2}{2m_N}\right)n + \vec{d}^{\,\dagger}\cdot\left(i\partial_0 + \frac{\nabla^2}{2m_d}\right)\vec{d} \\ &+ \sum_{j=1}^{2}\psi^{(j)\dagger}\left[\Delta_j + c_j\left(i\partial_0 + \frac{\nabla^2}{2M}\right)\right]\psi^{(j)} \\ &+ \sqrt{\frac{2\pi}{3\mu}}\left[\left(\psi^{(1)\dagger} + \psi^{(2)\dagger}\right)\vec{\sigma}\cdot n\vec{d} + \text{H.c.}\right] + \cdots . \end{aligned} \tag{3}$$

Here, n is the spin-doublet neutron field with mass m_N, $\vec{d}$ is the spin-triplet deuteron field with mass $m_d \approx 2m_N$, and $\psi^{(j)}$ with $j = 1, 2$ are two auxiliary spin-1/2 fields with total mass $M = m_N + m_d \approx 3m_N$ and residual masses Δ_j. $\vec{\sigma}$ are Pauli matrices that act on the (suppressed) spinor indices of n and $\psi^{(j)}$. We chose to fix the couplings of both auxiliary fields to neutron and deuteron in terms of the reduced mass μ, transferring their strength to parameters c_j [32]. In the power counting discussed below, $c_2 \ll c_1$ and the corresponding interaction appears at subleading orders together with the interactions lumped into the "$\cdots$". Integrating out $\psi^{(2)}$ one recovers the Lagrangian from Ref. [33], but the scaling of parameters is different here. Our approach inspired a reformulation of chiral EFT in the 2N $^1S_0$ channel where not only the shallow virtual state but also the amplitude zero is taken into account [34].

A straightforward calculation of the *nd* scattering amplitude $T_t(p)$ at LO in the halo EFT, where the contribution from the loops is resummed, gives

$$iT_t(p) = \frac{2\pi i}{\mu}\left[-\left(\frac{1}{\Delta_1 + c_1 p^2/(2\mu)} + \frac{1}{\Delta_2}\right)^{-1} - L(p)\right]^{-1}. \tag{4}$$

The loop contribution,

$$L(p) = 4\pi\int\frac{d^3\boldsymbol{q}}{(2\pi)^3}\frac{1}{q^2 - p^2 - i0^+} = ip\,, \tag{5}$$

was, for simplicity, evaluated in dimensional regularization using minimal subtraction. The final result is independent of the regularization method. We obtain the modified ERE (2) from Eq. (4) with

$$\begin{aligned} p_0^2 =& \frac{2\mu}{c_1}(\Delta_1 + \Delta_2)\,, \qquad & \frac{1}{a} =& A + R = \frac{\Delta_1\Delta_2}{\Delta_1 + \Delta_2}\,, \\ -\frac{r}{2} =& \frac{A}{p_0^2} = \frac{c_1}{2\mu}\frac{\Delta_2}{\Delta_1 + \Delta_2}\,, & & \end{aligned} \tag{6}$$

the shape-like parameter $s \propto B$ appearing at higher order.

4. Analysis

To develop a consistent power counting for the halo EFT, we start with the analytic structure of the T-matrix $T_t(p)$. The T-matrix poles here are the roots of

$$\begin{aligned} p\cot\delta - ip =& \frac{-1/a + rp^2/2}{1 + p^2/p_0^2} - ip \\ =& -i\frac{(p - i\kappa_1)(p - i\kappa_2)(p - i\kappa_3)}{p^2 + p_0^2}\,, \end{aligned} \tag{7}$$

with

$$\begin{aligned} \kappa_1 + \kappa_2 + \kappa_3 =& -\frac{r}{2}p_0^2 = A\,, \\ \kappa_1\kappa_2 + \kappa_2\kappa_3 + \kappa_3\kappa_1 =& -p_0^2\,, \quad \kappa_1\kappa_2\kappa_3 = -\frac{p_0^2}{a}\,. \end{aligned} \tag{8}$$

Using the parameters a, r, p_0 fitted earlier for $g_t = g_s = 1$, the three roots $i\kappa_1 \approx -27i$ MeV, $i\kappa_2 \approx 35i$ MeV, and $i\kappa_3 \approx 83i$ MeV are imaginary. As we move towards unitarity ($g_s = 0$, $g_t \to 0$), we refit the $\not\pi$EFT results with Eq. (7), as shown in Fig. 1. The roots remain imaginary. The third root is always deeper than the breakdown scale $\Lambda_b \sim \gamma_t$ of the halo EFT, and is, therefore, not relevant. We have checked that the position of the shallow poles change by at most a few percent when the shape-like parameter s (or B) is included, in agreement with the power counting.

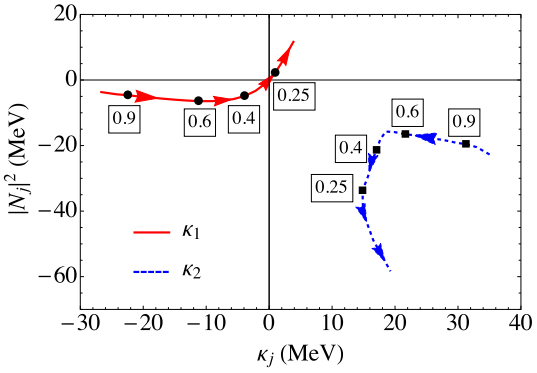

Fig. 2. Normalizations $|N_j|^2$ for the imaginary roots $i\kappa_1$ (red solid curve) and $i\kappa_2$ (blue dashed curve). The arrows indicate the evolution of the states as we make g_t smaller. A few g_t values are indicated as (black) circles on the κ_1 curve and as (black) squares on the κ_2 curve. The breakdown scale Λ_b gets smaller as $g_t \to 0$ and the redundant pole moves beyond the range of the halo EFT near the emergence of the excited state.

Near the poles we can write the S-matrix $S_t(p) = \exp[i2\delta(p)] \approx \sum_j R_j/(p - i\kappa_j) + f(p)$, where R_j are the residues at the poles, and $f(p)$ some finite piece. We provide an interpretation of the shallower roots based on the residues $R_{1,2}$. The wavefunction normalizations for the two shallowest poles are

$$|N_1|^2 = iR_1 = \frac{2\kappa_1(\kappa_1^2 - p_0^2)}{(\kappa_1 - \kappa_2)(\kappa_1 - \kappa_3)}\,,$$
$$|N_2|^2 = iR_2 = \frac{2\kappa_2(\kappa_2^2 - p_0^2)}{(\kappa_2 - \kappa_1)(\kappa_2 - \kappa_3)}\,, \qquad (9)$$

and their evolution towards unitarity is shown in Fig. 2. For a bound state, the normalization must be non-negative. At the physical point $g_t = g_s = 1$, the shallowest root $i\kappa_1$ with $\kappa_1 < 0$ is a pole on the second Riemann energy sheet with a negative normalization $iR_1 < 0$, and thus describes the virtual state that has been identified in the past [15]. The second root $i\kappa_2$ is a pole on the first energy sheet since $\kappa_2 > 0$. However, its normalization is also negative, $iR_2 < 0$ – it is a "redundant pole" [35,36] and does not describe a physical state. As we take the limit $g_t \to 0$ at $g_s = 0$, the second root $i\kappa_2$ remains a redundant pole and the first root $i\kappa_1$ evolves from a virtual to a real bound state.

In devising the power counting for the halo EFT, the three physical scales identified earlier, $|p_0| \sim Q$, $|\kappa_1| \sim \aleph$ and $\Lambda_b \sim \gamma_t$, have to be taken into account. The scale Q starts as the smallest, gets smaller in size and then grows. When $|p_0|$ grows beyond the breakdown scale, $|p_0| \gtrsim \Lambda_b$, it stops being relevant in halo EFT. We find it convenient to separate the evolution into three intervals of g_t to account for different relative sizes of Q. Moreover, as the modified ERE is most easily expressed in terms of the scattering parameters a, r, p_0 and s, we use these to write the power counting for the renormalized halo EFT couplings c_1, c_2, Δ_1 and Δ_2.

Initially, for $1 \gtrsim g_t \gtrsim 0.55$, we have $Q \ll \aleph \ll \Lambda_b$. The sizes of $|\kappa_1|$ and $|\kappa_2|$ are similar and we also identify $|\kappa_2| \sim \aleph$ to avoid introducing another scale. As we make g_t smaller, we find that κ_3 gets deeper while κ_1 gets shallower, so we take $\kappa_3 \sim A \sim \Lambda_b^2/\aleph$. These roots arise if the halo EFT couplings are large, $\Delta_{1,2} \sim \Lambda_b^2/\aleph$ and $c_1/(2\mu) \sim \Lambda_b^2/\aleph^3$, but with a cancellation in $\Delta_1 + \Delta_2 \sim \Lambda_b^2 Q^2/\aleph^3 \ll \Delta_{1,2}$. From Eq. (6) we see that p_0 comes out shallow as assumed, while $1/a \sim R \sim \aleph\Lambda_b^2/Q^2 \gg A$ and $r \sim \Lambda_b^2/(\aleph Q^2)$ are large. For $p \ll \aleph$, Eq. (7) is dominated by the a term containing the amplitude zero, and for $p \ll Q$ the effective range is $\sim 2(ap_0^2)^{-1}$. In contrast, for $p \gtrsim \aleph$ the r term and the unitarity term $(-ip)$ become comparable to the $1/a$ contribution and generate the T-matrix poles. If we take $c_2/(2\mu) \sim Q^2/\Lambda_b^3 \ll c_1/(2\mu)$, then the shape-like parameter $s = -(c_1c_2/\mu^2)/(\Delta_1 + \Delta_2) \sim 1/\Lambda_b^3$, which is consistent with its fit value at $g_t = 1$. Its contribution for $p \sim \aleph$ is suppressed by a factor of $sp^2/r \sim Q^2\aleph^3/\Lambda_b^5 \ll 1$ compared to the r and a contributions. Other modified ERE parameters appear at even higher orders. The halo EFT with the power counting we propose leads to a model-independent derivation of the modified ERE, and describes the data accurately.

As we make g_t smaller, p_0^2 gets smaller and changes sign such that $p\cot\delta$ develops a pole at real momentum around $g_t = 0.9$, analogous to the Ramsauer–Townsend effect [37,38]. This is shown in panel (b) of Fig. 1. The halo EFT (and the modified ERE) still gives a good description of the phase shift through the pole in $p\cot\delta$ even though the EFT couplings are fitted at momentum below the pole, as indicated in the figure. As g_t gets smaller, $|p_0^2|$ gets larger and we look at the second interval below.

For $0.55 \gtrsim g_t \gtrsim 0.35$, $|p_0|$ continues to grow, approaching and exceeding Λ_b. The first root is a progressively shallower virtual state with $\kappa_1 < 0$ and $iR_1 < 0$, while the second root stays a redundant pole with $\kappa_2 > 0$ and $iR_2 < 0$. Making $Q \to \Lambda_b$ in the relations of the first interval leads to $a \sim r \sim 1/\aleph$. Numerically, this works well. It can be accomplished with $\Delta_1 \sim \aleph$, $\Delta_2 \sim \Lambda_b^2/\aleph \gg \Delta_1$, and $c_1/(2\mu) \sim 1/\aleph$. From Eq. (4), one sees that the second auxiliary field contribution is suppressed by $\aleph^2/\Lambda_b^2$ at small momenta $p \sim \aleph$, and the modified ERE increasingly looks similar to the traditional ERE written as a Taylor series around $p = 0$. The situation is depicted in panel (c) in Fig. 1. With $c_2/(2\mu) \sim 1/\Lambda_b \ll c_1/(2\mu)$, the shape-like parameter contribution continues to be suppressed by $sp^2/r \sim \aleph^3/\Lambda_b^3 \ll 1$.

In the third interval, $0.35 \gtrsim g_t \gtrsim 0.1$, $|p_0| \sim Q$ becomes very large. The fits to $\not\pi$EFT scattering phase shift are not sensitive to p_0 which decouples from the theory. The S-matrix now has only two poles constrained by $\kappa_1 + \kappa_2 = 2/r$ and $\kappa_1\kappa_2 = 2/(ar)$, and two residues

$$|N_1|^2 = iR_1 = -\frac{4}{r}\frac{\kappa_1}{\kappa_1 - \kappa_2}\,,$$
$$|N_2|^2 = iR_2 = -\frac{4}{r}\frac{\kappa_2}{\kappa_2 - \kappa_1}\,. \qquad (10)$$

The first root continues to get smaller, and at around $g_t \simeq 0.3$ it vanishes. Then it moves to the first Riemann energy sheet as a real bound state with a positive normalization $iR_1 > 0$. The second root remains a redundant pole, and eventually moves slightly beyond the breakdown scale Λ_b. Near the emergence of the shallow bound state, the phase shift is characterized by a large scattering length and a small effective range, as seen in panel (d) of Fig. 1. Qualitatively, the phase shift goes from something similar to the ${}^1S_0$ 2N system with a shallow virtual state to the ${}^3S_1$ 2N channel with a shallow bound state. The scattering length scales as $|a| \sim 1/\aleph$ whereas the effective range r remains fixed at some other small momentum scale set by the second root, $\kappa_2 \sim \aleph' \sim 1/r \gg \aleph$. We did not explore how $\aleph'$ scales with variation of the nd input parameter a_3 (through $\Lambda_\star$) in $\not\pi$EFT. The halo EFT couplings scale as $\Delta_1 \sim \aleph$, $c_1/(2\mu) \sim 1/\aleph'$, and $\Delta_2 \to \infty$. The second auxiliary field is integrated out of the low-momentum theory, and we recover the traditional ERE. The shape-parameter contribution can be included in the single auxiliary-field formulation as a higher-order operator. With a scaling $s \sim 1/\Lambda_b^3$, the shape parameter is suppressed by $asp^4 \sim \aleph^3/\Lambda_b^3$ compared to the LO scattering-length contribution, whereas the effective-range correction is suppressed by $arp^2 \sim \aleph/\aleph'$.

The subsequent evolution of the new bound state is shown in Fig. 3, the "Efimov plot" calculated directly in $\not\pi$EFT. The physical triton at $g_t = g_s = 1$ is seen below the diagonal line on the

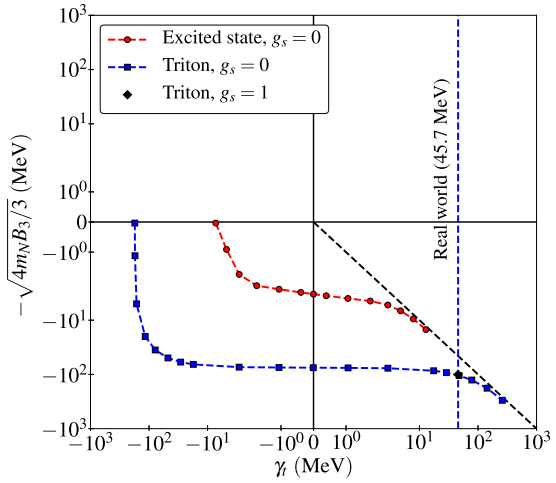

Fig. 3. Efimov states: the negative of the three-nucleon binding momentum ($-\sqrt{4m_N B_3/3}$) is plotted as a function of the deuteron binding momentum (γ_t), both in MeV. The diagonal dashed line in the fourth quadrant shows the threshold for breakup into neutron and deuteron. The physical value of γ_t is indicated by the vertical (blue) dashed line and the triton, by a (black) diamond. The evolution of the triton at ${}^1S_0$ unitarity ($g_s = 0$) is represented by the (blue) squares connected by a (blue) dashed line. The evolution of the first-excited state is represented by the (red) circles connected by a (red) dashed line.

fourth quadrant that marks the breakup threshold. For this bound state, there is no significant difference between $g_s = 0$ and $g_s = 1$ as the scaling violation due to nonzero $\gamma_s = 1/a_s \simeq -8$ MeV is a small effect compared to the binding momentum of the triton ~ 100 MeV [27]. As we move towards unitarity with $g_s = 0$, $g_t \to 0$, the new, shallow Efimov state appears around $g_t \simeq 0.3$. It occurs exactly at the place indicated earlier by the halo EFT based on the analytic structure of the S-matrix. We verified that the value of g_t where the excited state emerges changes by only a few percent at NNLO. The LO triton binding energy at this point is 5.5 MeV compared to 8.6 MeV at $g_t = 1$. At the unitarity point $g_t = 0$, the ratio of binding momenta between the triton and the first-excited state gives the geometric factor 22.7 predicted by Efimov [1–4].

Efimov physics displays a limit-cycle behavior [39,40], and shallower bound states (not shown in Fig. 3) also appear. For example, we have found that, as we evolve towards unitarity, around $g_t \simeq 0.05$ a new shallow virtual state is present and the phase shift goes through the same qualitative behavior as for the first excited state. Again a modified ERE with a new set of scattering parameters describes this virtual state, which becomes shallower, and finally emerges as the second-excited state of the triton. The same process repeats *ad infinitum* at progressively smaller g_t intervals.

5. Conclusions

We studied the relation between virtual state and bound Efimov level in a three-body system. We chose *nd* scattering in the spin-doublet channel as it had been shown to support a virtual state and a bound triton. The geometric scaling between bound states had not been observed in this system because deeper Efimov levels are beyond the range of applicability of any reasonable nuclear theory. We have demonstrated that a new shallow Efimov state emerges from the virtual state as we drive the system towards unitarity, as shown in Ref. [16] with a separable potential model. The shallow state displays the geometric scaling predicted by Efimov at unitarity, and we find evidence that the accumulation of shallow Efimov levels involve pulling in shallow virtual states from the second Riemann energy sheet to the first sheet. Though we consider a specific nuclear system, our results are universal to any three-body system of bosons or three- or more-state fermions with resonating zero-ranged two-body interactions, at least one of them supporting a two-body bound state. The linear combination of the nuclear amplitudes $A_{s,t}$ that supports Efimov states has the same properties as the amplitude for bosons [22]. Moreover, our argument is reversible and implies that an Efimov level turns into a virtual state as we move away from unitarity at positive scattering length. In addition to atomic systems near a Feshbach resonance, recent lattice QCD calculations, even at unphysical quark masses, provide another interesting scenario where in the presence of a strong magnetic field the 2N interaction is driven towards unitarity [41].

Recently it has been argued [42] that nuclear ground states beyond the deuteron are characterized by a momentum scale intermediate between the pion mass and the inverse 2N scattering lengths. In this case, nuclei are accessible through $\not\pi$EFT with an additional expansion around the unitarity limit of infinite 2N scattering lengths. The existence of a shallow virtual *nd* state that becomes the triton excited state supports this picture.

A low-energy halo EFT was formulated for a model-independent description of the transition of the shallow virtual to the shallow bound state. We studied the analyticity of the S-matrix on the complex energy plane in order to interpret the various poles that correspond to bound, virtual or redundant states. The halo EFT formulated here could be useful in the study of low-energy *pd* scattering, for example for the model-independent extraction of doublet ERE parameters from $\not\pi$EFT [43]. In halo EFT, the Coulomb interaction is simpler as *pd* is effectively a two-body system. The halo EFT could also be useful in the low-energy description of the reactions $d(n,\gamma)^3$H and $d(p,\gamma)^3$He, which are relevant in big-bang nucleosynthesis.

Acknowledgments

The authors acknowledge many helpful conversations with Sebastian König and Jared Vanasse who also provided their triton amplitude values for benchmarking our three-body codes, and the stimulating environment of the IIP program “Weakly Bound Exotic Nuclei” where this project started. GR and UvK thank the Institute of Physics at the University of São Paulo, the Institute for Nuclear Theory at the University of Washington, the Kavli Institute of Theoretical Physics at the University of California Santa Barbara, and the ExtreMe Matter Institute at the Technical University, Darmstadt, for the kind hospitality while this research was carried out. GR acknowledges partial support from the Joint Institute for Nuclear Physics and Applications at Oak Ridge National Laboratory and the Department of Physics, University of Tennessee, during his sabbatical where part of this research was completed. This work was supported in part by FAPESP grant 2012/50984-4 (RH), project INCT-FNA Proc. No. 464898/2014-5 (RH), U.S. NSF grant PHY-1615092 (GR), the U.S. Department of Energy, Office of Science, Office of Nuclear Physics, under award No. DE-FG02-04ER41338 (UvK), the European Union Research and Innovation program Horizon 2020 under grant agreement No. 654002 (UvK), and CNRS’s Laboratoire International Associé France–Brésil “Subatomics” (RH and UvK).

References

[1] V.N. Efimov, Phys. Lett. B 33 (1970) 563.
[2] V.N. Efimov, Sov. J. Nucl. Phys. 12 (1971) 589.
[3] R.D. Amado, J.V. Noble, Phys. Lett. B 26 (1971) 25.
[4] R.D. Amado, J.V. Noble, Phys. Rev. D 5 (1972) 1992.
[5] T. Kraemer, et al., Nature 440 (2006) 315.
[6] S. Knoop, et al., Nat. Phys. 5 (2009) 227.

[7] M. Zaccanti, et al., Nat. Phys. 5 (2009) 586.
[8] N. Gross, Z. Shotan, S. Kokkelmans, L. Khaykovich, Phys. Rev. Lett. 103 (2009) 163202.
[9] B. Huang, L.A. Sidorenkov, R. Grimm, J.M. Hutson, Phys. Rev. Lett. 112 (2014) 190401.
[10] M. Kunitski, et al., Science 348 (2015) 551.
[11] A.S. Jensen, K. Riisager, D.V. Fedorov, E. Garrido, Rev. Mod. Phys. 76 (2004) 215.
[12] T. Frederico, A. Delfino, L. Tomio, M.T. Yamashita, Prog. Part. Nucl. Phys. 67 (2012) 939.
[13] H.W. Hammer, C. Ji, D.R. Phillips, J. Phys. G 44 (2017) 103002.
[14] W.T.H. van Oers, J.D. Seagrave, Phys. Lett. B 24 (1967) 562.
[15] B.A. Girard, M.G. Fuda, Phys. Rev. C 19 (1979) 579.
[16] S.K. Adhikari, A.C. Fonseca, L. Tomio, Phys. Rev. C 26 (1982) 77.
[17] M.T. Yamashita, T. Frederico, L. Tomio, Phys. Lett. B 660 (2008) 339.
[18] M.T. Yamashita, T. Frederico, L. Tomio, Phys. Lett. B 670 (2008) 49.
[19] M.A. Shalchi, M.T. Yamashita, M.R. Hadizadeh, E. Garrido, L. Tomio, T. Frederico, Phys. Rev. A 97 (2018) 012701.
[20] J.-W. Chen, G. Rupak, M.J. Savage, Nucl. Phys. A 653 (1999) 386.
[21] X. Kong, F. Ravndal, Nucl. Phys. A 665 (2000) 137.
[22] P.F. Bedaque, H.W. Hammer, U. van Kolck, Nucl. Phys. A 676 (2000) 357.
[23] G. Rupak, Nucl. Phys. A 678 (2000) 405.
[24] H.W. Hammer, T. Mehen, Phys. Lett. B 516 (2001) 353.
[25] P.F. Bedaque, G. Rupak, H.W. Griesshammer, H.-W. Hammer, Nucl. Phys. A 714 (2003) 589.
[26] J. Vanasse, Phys. Rev. C 88 (2013) 044001.
[27] S. König, H.W. Grießhammer, H.-W. Hammer, U. van Kolck, J. Phys. G 43 (2016) 055106.
[28] C.A. Bertulani, H.W. Hammer, U. van Kolck, Nucl. Phys. A 712 (2002) 37.
[29] P.F. Bedaque, H.W. Hammer, U. van Kolck, Phys. Lett. B 569 (2003) 159.
[30] U. van Kolck, Nucl. Phys. A 645 (1999) 273.
[31] W. Dilg, L. Koester, W. Nistler, Phys. Lett. B 36 (1971) 208.
[32] H.W. Griesshammer, Nucl. Phys. A 744 (2004) 192.
[33] D.B. Kaplan, Nucl. Phys. B 494 (1997) 471.
[34] M. Sánchez Sánchez, C.J. Yang, B. Long, U. van Kolck, Phys. Rev. C 97 (2018) 024001.
[35] S.T. Ma, Phys. Rev. 71 (1947) 195.
[36] R.J. Eden, J.R. Taylor, Phys. Rev. 133 (1964) B1575.
[37] C.W. Ramsauer, Ann. Phys. 64 (1921) 513.
[38] J.S. Townsend, V.A. Bailey, Philos. Mag. 43 (1922) 593.
[39] P.F. Bedaque, H.W. Hammer, U. van Kolck, Phys. Rev. Lett. 82 (1999) 463.
[40] P.F. Bedaque, H.W. Hammer, U. van Kolck, Nucl. Phys. A 646 (1999) 444.
[41] W. Detmold, K. Orginos, A. Parreno, M.J. Savage, B.C. Tiburzi, S.R. Beane, E. Chang, Phys. Rev. Lett. 116 (2016) 112301.
[42] S. König, H.W. Grießhammer, H.-W. Hammer, U. van Kolck, Phys. Rev. Lett. 118 (2017) 202501.
[43] S. König, H.W. Grießhammer, H.W. Hammer, J. Phys. G 42 (2015) 045101.